Antiferromagnetism beyond the classical percolation threshold in the diluted half-filled one-band Hubbard model in three dimensions

Sourav Chakraborty,[1] Anamitra Mukherjee,[2,*] and Kalpataru Pradhan[1,†]
[1]*Theory Division, Saha Institute of Nuclear Physics, A CI of Homi Bhabha National Institute, Kolkata-700064, India*
[2]*School of Physical Sciences, National Institute of Science Education and Research, A CI of Homi Bhabha National Institute, Jatni 752050, India*

(Received 20 December 2021; revised 31 May 2022; accepted 15 August 2022; published 26 August 2022)

We investigate the impact of dilution by setting the on-site repulsion strength U to zero at a fraction of sites in the half filled Hubbard model on a simple cubic lattice. We employ a semiclassical Monte Carlo approach first to recover the zero dilution (undiluted $x = 1$) properties, including U dependence of insulator to metal crossover temperature scale T^* and long-range staggered antiferromagnetic ordering temperature T_N. For the nonperturbative regime of $U \approx$ bandwidth, we find a rapid suppression of T^* with reducing x from 1 to 0.7. However, T_N remains unchanged in this dilution range, showing a weakening of the insulating state but not of the magnetic order. At $x \leqslant 0.7$, T^* and T_N coincide and are suppressed together with decrease in x. Within the Monte Carlo study we show that the long-range magnetic order vanishes at $x = 0.15$ at $T = 0.01$ much below the classical percolation threshold. The magnetic order below the classical percolation threshold is in line with the expected fragile long-range magnetic order at vanishingly small x at $T = 0$. We exhibit that the induced moments on $U = 0$ sites drive the magnetic order below the classical percolation limit by studying local moment systematics and finite-size analysis of magnetic order. At the end, we show that either increasing U to large values or raising temperature beyond a U dependent critical value, suppresses the induced local moments of the $U = 0$ sites and recovers the classical percolation threshold.

DOI: 10.1103/PhysRevB.106.075146

I. INTRODUCTION

The discovery of high-temperature superconductivity in doped copper oxides generated an enormous amount of interest in quantum antiferromagnets [1–3]. The emergence and collapse of long-range antiferromagnetic (AF) order, which provides us a unique way to explore many exotic magnetic phases, is one of the most well-explored topics in condensed-matter physics. The AF ordering in cuprates, iron-pnictides, and iron-chalcogenides gets suppressed by doping nonmagnetic impurities [4–6]. Spin-wave theory for a low concentration of impurities with the impurities treated as static vacancies [7,8] can usually model such behavior. On the other hand, frustration arising from in-plane couplings in clean systems can also disrupt long-range magnetic order (LRO) and are routinely explored within the $J_1 - J_2$ Heisenberg spin models [9–11]. Vacancy-based disorder induces suppression of long-range magnetic order [12,13] and have been typically studied in the strong-coupling limit. Quantum Monte Carlo simulations [14] in the large correlation strength limit, agree with the AF order vanishing at the classical percolation threshold as in the experiments.

Cuprates like $La_2Cu_x(Mg/Zn)_{1-x}O_4$ [15–18] have inspired some diluted Hubbard model studies in two and quasi-two dimensions [17,19–21]. While there are materials complications (for example Zn doping leads to a local on-site potential different from the Cu sites, but Coulomb repulsion at Zn sites should not be neglected completely) the spirit of the theoretical modeling in the literature cited above is that of understanding dilution effects in a quantum magnet in simple models. The experimental motivation was to investigate superconductivity in the parent material (La_2CuO_4) by doping with nonmagnetic Zn or Mg that suppresses long-range antiferromagnetic order. According to the current understanding this quasi-two-dimensional (quasi-2D) material [$La_2Cu_x(Mg/Zn)_{1-x}O_4$] shows complete suppression of long-range AF order [18] for $x_p^{2D} \approx 0.59$, the classical percolation threshold [14,22]. In the strong-interaction limits for such materials where $3d$ transition-metal elements are involved [14,23–25], the long-range magnetic order vanishes at x_p, the critical classical percolation threshold in the relevant dimensions.

However, investigations of dilution for the Hubbard model where U is comparable to the bandwidth (BW) are relevant both for materials and are of theoretical interest. In particular, since the correlation-induced suppression of double occupation is not too severe, sites with $U = 0$ in vicinity of $U \neq 0$ sites can get nontrivially effected by virtual charge fluctuations leading to induced moments on the uncorrelated sites. Thus, whether diluting the correlated sites will suppress the long-range antiferromagnetic order of the undiluted system is unclear. Ulmke *et al.* [19] have shown that the long-range antiferromagnetic order vanishes at $x_c = 0.5$ which is smaller than x_p^{2D}. A recent study of the diluted Hubbard model on Lieb lattice also shows that the magnetic order is very robust for dilution much lower than the classical percolation threshold [26]. We note that at $T = 0$, percolation is expected to support fragile long-range order even for vanishingly small

*anamitra@niser.ac.in
†kalpataru.pradhan@saha.ac.in

x due to quantum effects. Thus the result of going below classical percolation threshold in finite-T calculations as performed in literature [19,26] as well in the present paper, are in conformity with the expected percolation at $T = 0$ with long-range order can occur even as $x \to 0$.

In the present work we focus on understanding the interplay of dilution and temperature in a simple model of strong correlation in a three-dimensional (3D) lattice. In 3D, long-range magnetic order can be stabilized free of Mermin-Wagner [27] issues that impede long-range order in 2D. In addition, due to the increase of coordination number, the percolation below classical percolation threshold is more robust. Hence, we analyze the effect of dilution in a Hubbard model at half filling on a simple cubic lattice using a semiclassical Monte Carlo (s-MC) scheme [28,29].

Our method reduces to an unrestricted Hartree-Fock method at very low temperatures but becomes progressively accurate with temperature increase and, in particular, compares well with determinant quantum Monte Carlo (DQMC) over a wide temperature range. We consider the half filled Hubbard model as defined below in three dimensions. We first produce several benchmarks for the undiluted case, including the AF magnetic order and its temperature dependence, local moment systematic and the related metal insulator crossover scale T^*. We then show that switching off interaction potential on a fraction of sites weakens and eventually destroys the magnetic order. However, remarkably, for correlation strength, where the bandwidth (BW) and interaction strength U are comparable, we show that the AF order survives to dilutions much below the classical percolation threshold. We investigate this phenomenon by tracking the local moment dependence with temperature. We show that $U \neq 0$ sites induce significant suppression of double occupation on the $U = 0$ sites stabilizing local moments on the uncorrelated sites.

In addition our calculations reveal that the density of states carries the signature of this effect and manifests as a four-lobe Mott insulator. At a critical dilution below the classical threshold, we show that the collapse of local moments at the $U = 0$ sites signals the onset of a metallic state. We find that the ensuing metal has a pseudogapped density of states at low temperatures. Finally, we demonstrate that the vanishing of the AF order at the classical percolation threshold occurs for U much larger than the BW, in agreement with earlier literature. We also find that the same can happen at increased temperatures where thermal fluctuations destroy the local moments on the $U = 0$ sites. Thus we present a complete phenomenology within our semiclassical approach to analyze the interplay of dilution effects, correlation strength, and temperature.

II. MODEL AND METHOD

We consider the following particle-hole symmetric form of the one band Hubbard Hamiltonian:

$$H = -t \sum_{\langle i,j\rangle,\sigma} (c^\dagger_{i\sigma} c_{j\sigma} + \text{H.c.}) + U \sum_i \left(n_{i\uparrow} - \frac{1}{2}\right)\left(n_{i\downarrow} - \frac{1}{2}\right) - \mu \sum_i n_i, \quad (1)$$

where $c_{i\sigma}$ ($c^\dagger_{i\sigma}$) are the fermion annihilation (creation) operators at site i with spin σ. t is the nearest-neighbor hopping parameter and U (>0) denotes the on-site repulsive Hubbard interaction. μ is the chemical potential.

To employ the s-MC approach we decompose the on-site interaction term by introducing standard Hubbard-Stratonovich (HS) auxiliary fields (a vector field $\boldsymbol{m}_i$ that couples to spin degree of freedom while a scalar field ϕ_i couples to charge degree of freedom) at each site i. We treat auxiliary fields as *classical fields* by dropping the time dependence explicitly. We treat ϕ_i at the saddle-point level $i\phi_i = \frac{U}{2}\langle n_i\rangle$, but retain the thermal fluctuations for $\boldsymbol{m}_i$. These thermal fluctuations are necessary to capture many of the well established features which will be discussed later. The following effective spin-fermion Hamiltonian is derived using above approximations (see Appendix for the details and justification of the approximation):

$$H_{\text{eff}} = -t \sum_{\langle i,j\rangle,\sigma} (c^\dagger_{i\sigma} c_{j\sigma} + \text{H.c.}) + U/2 \sum_i (\langle n_i\rangle n_i - \mathbf{m}_i.\sigma_i) + (U/4) \sum_i \left(\mathbf{m}_i^2 - \langle n_i\rangle^2\right) - \frac{U}{2} \sum_i n_i - \mu \sum_i n_i.$$

We solve H_{eff} by using exact diagonalization based Monte Carlo method. We diagonalize the Hamiltonian for a fixed set of $\{\mathbf{m}_i\}$ and $\{\langle n_i\rangle\}$ configuration. We update the $\{\mathbf{m}_i\}$ at each site based on usual Metropolis scheme at a fixed temperature. The $\langle n_i\rangle$ fields are self-consistently updated at every 10th Monte Carlo step where the $\mathbf{m}_i$ fields are held fixed. We note that while particle-hole symmetry at half filling fixes the μ, in H_{eff}, the μ is calculated as a consistency check during the Monte Carlo annealing process containing thermal noise in the $\{\mathbf{m}_i\}$ fields. The goal of the process is to generate equilibrium configuration of the $\mathbf{m}_i$ and the $\langle n_i\rangle$ fields. Expectation values of observables are obtained by appropriately using the eigenvectors and eigenvalues resulting from diagonalizing the Hamiltonian in each of the equilibrium configuration. These individual expectation values from equilibrium configurations are further averaged over results from 100 such configurations at a fixed temperature. All observables are calculated at a given temperature by averaging over the values obtained from individual configurations. We note that we calculate observables from every tenth equilibrium configuration to avoid spurious self correlations. Temperature is lowered in small steps to allow for equilibration. To avoid size limitation we employ above-mentioned Monte Carlo technique within a traveling-cluster approximation [30–32] to handle system size $N = L^3 = 10^3$.

For $0 < x < 1$, we have Nx fraction of sites with finite U and $N(1-x)$ sites with $U = 0$, with N being the total number of sites. For $U = 8$, on-site interactions U_i at each sites are chosen using the distribution $P(U_i) = (1-x)\delta(U_i) + x\delta(U_i - 8)$. We introduce the HS auxiliary fields only on the $U \neq 0$ sites. But, the induced moments on the $U = 0$ sites are calculated by computing quantum local moments, as we discuss later. We would like to emphasize that in the particle-hole symmetric Hubbard model an additional $-U/2$ potential exists at all sites, which is a uniform onsite potential over the entire system. When removing a correlated site, this additional on-site potential is also removed, thereby creating a strong on-site potential on the $U = 0$ sites. All our results pertain to this simple particle-hole symmetric case. A more realistic

modeling would be to explicitly add a local potential on the $U = 0$ sites, which in our case is always set to zero upon dilution. In addition to thermal averaging discussed above all physical quantities are averaged over ten different random configurations of onsite potentials. Finally, all energy scales (U, temperature, BW, etc.) are measured in units of the hopping parameter t.

III. PHASE DIAGRAM

Before moving to the diluted case, let us briefly summarize the physics of the $x = 1$ case from literature. The half filled Hubbard model has been studied extensively with a plethora of numerical techniques such as determinantal quantum Monte Carlo (DQMC) [33], dynamical mean-field theory (DMFT) [34] and its cluster versions, dynamical cluster approximation (DCA) [35], and cluster-DMFT (C-DMFT) [36]. At half filling in 2D DQMC indicates an insulating ground state at all $U > 0$ and the system show G-type (staggered) antiferromagnetic correlations. The Néel temperature T_N shows a nonmonotonic behavior with U and there is a regime of preformed local moments above the magnetic order which terminates at T^*, above which the system is a paramagnetic metal. The system shows a pseudogapped phase with increase in temperature whereby the $T = 0$ Mott gap is gradually filled up [37]. In single site DMFT, only a paramagnetic solution is possible and technically it is in the limit of infinite coordination. It shows that the Mott transition in the U-T plane is first order in nature. The first-order line is ending at a finite-temperature critical point. It also predicts coexistence of the metallic and insulating phases. Cluster variants such as C-DMFT modifies this picture by the addition of short-range correlation effects. However, the main features of the single-site DMFT picture are not affected, except that the critical line changes slope from negative to positive [38]. More recent 2D C-DMFT [39] work also finds a similar trend of T_N with U as DQMC. They carefully try to elucidate the difference between weak and strong U insulating ground states and argue that the normal state just above T_N controls the difference between weakly and strongly interacting antiferromagnetic states. In particular, they show that the small-U antiferromagnetic state arises upon cooling a metal, while the large-U antiferromagnet is established by cooling a Mott insulator. They also infer a first-order normal-metal to Mott transition at low T (if antiferromagnetism is suppressed) with increasing U. A detailed magnetic phase diagram study of the half filled one band Hubbard model using finite-temperature scheme of variational cluster approximation (VCA) in two dimensions by Seki *et al.* [40] also agrees well with the C-DMFT results [41].

In 3D cluster-DMFT with incorporating vertex corrections it has been shown that T_N varies nonmonotonically with U, similar to DQMC results [42]. The resulting antiferromagnetic phase diagram of the three-dimensional Hubbard model at half filling using C-DMFT agrees quite well with quantum Monte Carlo (QMC) simulations [43] and the DCA calculations [44].

Next, we discuss briefly about the U-T phase diagram, seen in the inset of Fig. 1, obtained from our calculations for $x = 1$ (i.e., the undiluted case, without any $U = 0$ sites). We first find that, for all U, we have a staggered AF insulating

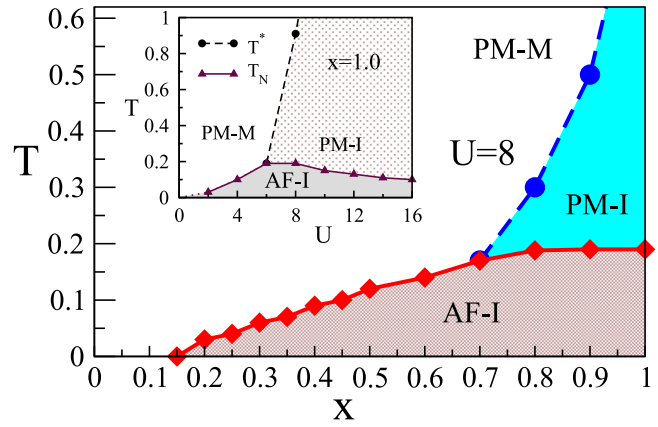

FIG. 1. x-T phase diagram for $U = 8$. x is the concentration of correlated sites ($U = 8$) and rest of the sites (with concentration $1 - x$) have $U = 0$. PM-I phase intervenes between the PM-M and AF-I phase for $x > 0.7$. For $x \leqslant 0.7$ the PM-I phase vanishes and the metal insulator transition coincides with the onset of the AF order. For $x \leqslant 0.15$ the AF order completely collapses at low temperatures. The inset shows the U-T phase diagram. For details please see the text.

ground state (AF-I). The staggered AF transition temperature T_N defines the finite-temperature boundary of the AF and the PM phase. The antiferromagnetic transition temperature T_N increases with U up to $U = 8$ and decreases thereafter. For larger U, s-MC captures $\approx t^2/U$ scaling of T_N. In the inset we also find that, for large U above T_N, there is an insulating region of preformed local moments with no long-range magnetic order (PM-I). This phase crosses over to a paramagnetic metal (PM-M) above the dashed line. We discuss below how these phases are determined for different values of x. For the $x = 1$ case, the nonmonotonic U dependence of T_N and the preformed local moment regime at finite temperature are results beyond simple finite temperature Hartree-Fock mean-field theory. Details and comparison with DQMC are presented in earlier s-MC literature [28]. s-MC has also been used to study the physics of the Anderson-Hubbard model [45] and the frustrated Hubbard model [46,47].

As mentioned in the introduction, our main motivation is to examine if the AF order can survive below the classical percolation threshold. For this we initially confine to $U = 8$, where T_N is optimum and study the effect of dilution. This value of U is away from the two perturbative limits of $U/BW \ll 1$ and $U/BW \gg 1$. We will discuss the systematics of varying U at a later stage. The main panel in Fig. 1, shows the x-T phase diagram for $U = 8$. We see that the T_N (diamonds) and crossover scale (dashed line) both decrease as x is reduced. Within numerical accuracy, the PM-I phase exists for $x > 0.7$. The important observation is that the T_N survives up to $x = 0.15$, much smaller than the classical three-dimensional percolation threshold ($x_p^{sc} \approx 0.31$). We will show below that this conclusion is robust to changes in the system size.

IV. MAGNETIC AND TRANSPORT PROPERTIES

Next we discuss the magnetic and transport properties in details that we use to construct the phase diagram for diluted Hubbard model (Fig. 1).

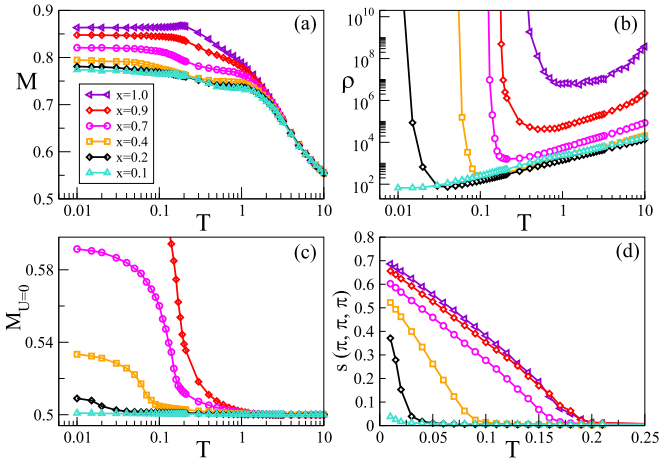

FIG. 2. Physical quantities for different x values. All calculations are done for $U = 8$ unless otherwise specified. (a) Average local moments M vs temperature measured using only $U = 8$ sites. (b) Resistivity vs temperature curves for different x values. (c) The induced moments with temperature specifically at $U = 0$ sites. Legends are same in panels (a)–(d). (d) Quantum structure factor $s(\pi, \pi, \pi)$ vs temperature (by taking $U = 8$ sites only) for different x. With decrease in x the quantum structure factor decreases at low temperature. The Néel temperature T_N also decreases and vanishes for $x = 0.1$.

Metal-insulator transition and magnetic order. From the $x = 1$ analysis we know that local moments exist on all sites for $U = 8$. For $x = 1$ the system averaged $M_z^2 = \langle (n_\uparrow - n_\downarrow)^2 \rangle = \langle n \rangle - 2\langle n_\uparrow n_\downarrow \rangle$, which is the square of the quantum local moment, where the angular brackets imply quantum and thermal averaging at individual sites. Following the literature [37], we calculate this observable $M \equiv M_z^2$ to infer about local moment systematics. The large moment at low temperature is due to the increased suppression of doublons (local double occupation). In the limit $U \to \infty$ and at any finite temperature we expect the double occupation to decrease drastically, but virtual excitations would not allow it to go to zero for giving a perfect $M = 1$ result. In the other extreme limit of $U = 0$ or $T \to \infty$ at any finite U, the double occupation $\langle n_\uparrow n_\downarrow \rangle \to \langle n_\uparrow \rangle \langle n_\downarrow \rangle = 0.25$. This gives the value of M to be 0.5 at half filling. In Fig. 2(a) we show the local moment M vs temperature data for various x values for the $U \neq 0$ sites. For $x = 1$, this of course coincides with the system averaged local moments, while for $x \neq 1$, the site averaging is done only over the $U \neq 0$ sites.

To understand the actual temperature scale for moment formation that lies between these two limits and its impact on transport properties we calculate the resistivity as function of temperature in Fig. 2(b). Resistivity is calculated for different x values by calculating the *dc* limit of the optical conductivity determined by the Kubo-Greenwood formula [48,49]. A metal-insulator crossover (MIC) scale (T^*) is ascertained from the change in the sign of $d\rho/dT$. For $x = 1$, and $U = 8$, $T^* \approx 1$. For the $x < 1$ case we see that this crossover scale reduces rapidly. To understand this systematics, let us analyze the local moments of the correlated $U \neq 0$ [plotted in Fig. 2(a)] and uncorrelated ($U = 0$) sites [plotted in Fig. 2(c)] separately. For the correlated sites we see that there is an overall reduction in the local-moment magnitudes, but there is no drastic local moment collapse to suggest a significantly smaller MIC temperature, as the resistivity data suggest. However, the remarkable effect on deciding the scale for onset of metallicity with temperature increase comes from the $U = 0$ sites! In Fig. 2(c), we see that weak local moments are induced on the uncorrelated sites. We observe that T^* is controlled by the onset temperature of the local moments formation (M becoming greater than 0.5) on the uncorrelated sites. For example, for $x = 0.9$, the local moments of the correlated sites are similar in magnitude to the $x = 1$ case, yet the resistivity data show an insulator-to-metal crossover occurs at $T^* \approx 0.5$ as opposed to ≈ 1 for $x = 1$ case. We also notice that the onset of magnetic moments on $U = 0$ sites, transition from PM-M to AF-I phase occurs at same temperature for $x \leqslant 0.7$. This clear correlation needs the following clarification: whether the small moments on the $U = 0$ sites, for example, small moments very close to the uncorrelated value of 0.5 for $x < 0.4$, are responsible for stabilizing the low-temperature antiferromagnetic insulating state? In particular, is there a long-range order arising out of the sites with two values of local moments?

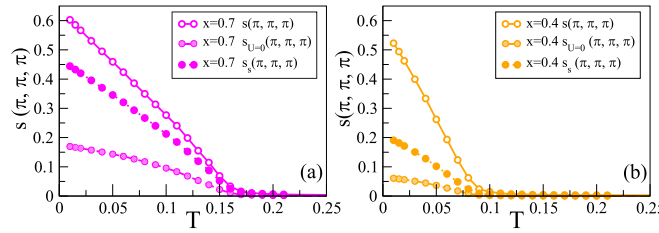

FIG. 3. Comparison of structure factors calculated using only $U = 8$ sites [$s(\pi, \pi, \pi)$], only $U = 0$ sites [$s_{U=0}(\pi, \pi, \pi)$] and using both $U = 8$ and $U = 0$ sites [$s_s(\pi, \pi, \pi)$]. Structure factor by taking both $U = 0$ and $U = 8$ sites [$s_s(\pi, \pi, \pi)$] vs temperature shows that the system as a whole turns antiferromagnetic at the same temperature to that of $U = 8$ sites [plotted using $s(\pi, \pi, \pi)$]. For comparison $s_{U=0}(\pi, \pi, \pi)$, calculated only for $U = 0$ sites, shows the transition at same temperature for (a) $x = 0.7$ and (b) $x = 0.4$.

To answer this question, in Fig. 2(d) we plot the quantum antiferromagnetic correlations $s(\pi, \pi, \pi)$ [$s(\mathbf{q}) = \frac{1}{(Nx)^2} \sum_{mn} \langle \mathbf{s}_m \cdot \mathbf{s}_n \rangle e^{i\mathbf{q}\cdot(r_m - r_n)}$ where $\mathbf{q}$ is the wave vector], where angular brackets have the same meaning as mentioned above and the indices $\{m, n\}$ run over only the $U = 8$ sites. The normalization is defined accordingly. The reduction in the T_N as well as the low-T saturation value with decreasing x is apparent. The weakening of antiferromagnetism due to the dilution is expected. However, we find an unexpected behavior when comparing the above with magnetic structure factor computed only for the $U = 0$ sites [denoted as $s_{U=0}(\pi, \pi, \pi)$]. In Fig. 3 we show two such comparisons for (a) $x = 0.7$ and (b) $x = 0.4$. The AF order that results from the $U = 0$ sites by itself generates long-range staggered AF correlations in three dimensions. Furthermore, the AF order from the two set of sites (taking $U = 8$ and $U = 0$ sites separately) and AF correlations $s_s(\pi, \pi, \pi)$ obtained by taking all the sites (both $U = 8$ and $U = 0$ sites at the same time) vanish at the same temperature. This shows the cooperation between the $U \neq 0$ and $U = 0$ sites that helps to commence the global antiferromagnetic correlation at that temperature.

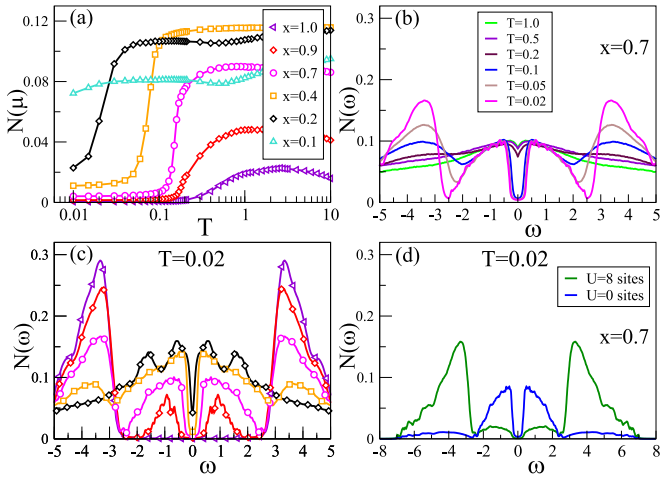

FIG. 4. (a) Temperature dependence of density of states at the Fermi energy $N(\mu)$ shows that the Mott gap collapses at high temperature due to thermal fluctuation. Thermal fluctuation persists up to low enough temperature for lower x values. $N(\mu)$ more or less remains constant with temperature for $x = 0.1$. (b) Density of states $N(\omega)$ with ω for different temperatures at $x = 0.7$. (c) Density of states $N(\omega)$ with ω for different x at $T = 0.02$. Legends are same in panels (a) and (c). For $x = 1$, the Mott gap at $T = 0.02$ shows Mott lobes around $\pm U/2$. A pair of secondary Mott lobe forms near $\omega = 0$ for $x < 1$. (d) U-dependent density of states for $x = 0.7$ shows that the secondary lobes are mainly due to the $U = 0$ sites.

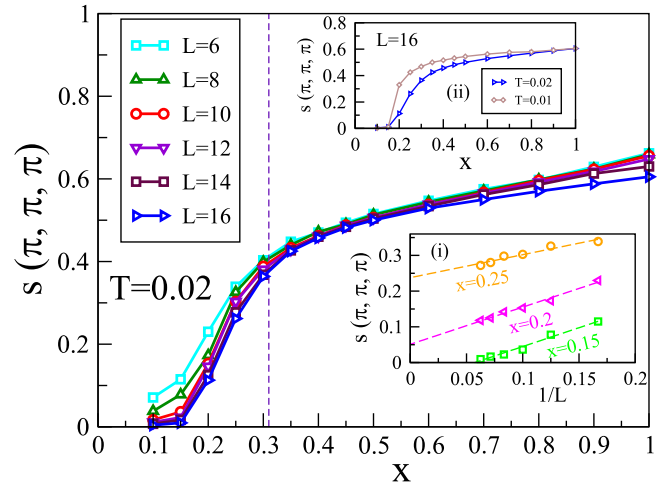

FIG. 5. Shows the drop of $s(\pi, \pi, \pi)$ with decrease in x values for different L values ($N = L^3$). For $T = 0.02$ long-range AF order persists up to $x = 0.15$. This AF order is due to the induced moment formed at $U = 0$ sites as explained in the text. The result is almost indistinguishable beyond system size 10^3. All calculations are done for $U = 8$. Inset (i) shows the $s(\pi, \pi, \pi)$ vs $1/L$ for $x = 0.15, 0.2$ and 0.25. Inset also shows linear fitting of $s(\pi, \pi, \pi)$ with $1/L$ for $x = 0.15$, 0.2 and 0.25. Inset (ii) shows that the long-range AF order also persists up to $x = 0.15$ for $T = 0.01$.

In addition, for $x \leqslant 0.7$, we find that the insulating state and the T_N coincide, reminiscent of a Slater like insulator. For $x > 0.7$, the data suggests that the insulting state can survive without the magnetic order, but requires finite local moments at the $U = 0$ sites. This is the continuation of the $x = 1$ PM-I phase for $x < 1$.

Density of states. In Fig. 4(a) we show the temperature evolution of the density of states at the chemical potential $N(\omega = \mu)$ for different values of x. Density of states are obtained by implementing the Lorentzian representation of the δ function in $N(\omega) = \sum_k \delta(\omega - \omega_k)$, where ω_k are the eigenvalues of the fermionic sector and the summation runs up to $2L^3$, i.e., the total number of eigenvalues of a L^3 system. The expected gradual filling up of the charge gap in the Mott state seen for $x = 1$ (see Ref. [37]) is also seen for smaller x values. The gap filling however becomes abrupt for $x \leqslant 0.7$. This is the same dilution below which we have a direct transition from a PM-M to an AF-I. In addition, the density of states are plotted explicitly for $x = 0.7$ in Fig. 4(b) at different temperatures. While not explored herein detail, overall the data suggests a possible first-order transition for $x \leqslant 0.7$. Finally for $x = 0.1$, we have a gap-less ground state.

The density of states are compared for different x values at low temperature $T = 0.02$, in Fig. 4(c). We see that with reducing x, the upper and lower Hubbard sub-bands around $\pm U/2$ evolves in to a four sub-band structure and the gap around chemical potential μ ($\omega = 0$) reduces. The gap eventually closes and we find a pseudogapped metal for $x = 0.1$. To understand the origin of the new features in the density of states we show the contribution of the density of states from $U = 0$ and $U = 8$ sites separately in Fig. 4(d) for $x = 0.7$ at the same low temperature. It shows that $U = 0$ sites mostly contribute to the formation of the low-energy Mott lobes (around $\omega = \pm 1$). This four sub-band density of states within s-MC qualitatively agrees with DQMC [19].

V. PERCOLATION THRESHOLD

To start with, we first demonstrate the stability of the critical percolation threshold obtained from finite-size lattices. Since the AF order parameter is the central indicator used by us, in Fig. 5 we show the low-temperature value of $s(\pi, \pi, \pi)$ for different system sizes as a function of x. The system size is defined as L^3. Beyond 10^3 the results for low x are barely distinguishable from each other. We see from the data that the order parameter rapidly converges with system size, giving the limiting value of $x_p = 0.15$. The inset (i) shows $s(\pi, \pi, \pi)$ plotted as a function of inverse system size ($1/L$) for three values of x. We find that, for $x > 0.15$, $s(\pi, \pi, \pi)$ saturates to a finite value for $L \to \infty$, while it approaches zero for $x = 0.15$. This analysis shows that indeed in the thermodynamic limit the AF order survives below the classical percolation threshold $x_p^{sc} \approx 0.31$. Inset (ii) shows that the long-range AF order also persists up to $x = 0.15$ for $T = 0.01$. Below this temperature the magnetic order for small x is very weak and beyond our numerical calculations. Nonetheless, in principle at $T = 0$ the quantum percolation should occur at arbitrarily small x. However, such a magnetic order will be extremely fragile to thermal fluctuations. To clarify the nature of the antiferromagnetic order below the $x_p^{sc} \approx 0.31$, in Fig. 6(a) we present the distribution of local moments in real space that includes both the $U = 0$ and $U = 8$ sites at $T = 0.02$. The local-moment distribution $P_q(M) = \sum_{M_i} \delta(M - M_i)$ shows two peaks. In the limiting case of $x = 1$ the expected plot is that of a single

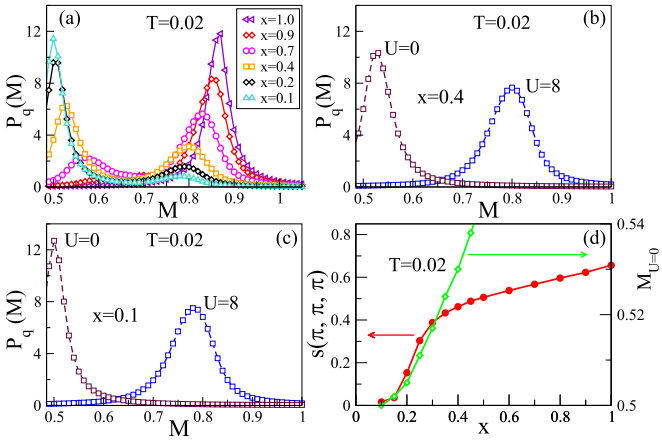

FIG. 6. (a) Distribution of local moments by taking both $U = 8$ and $U = 0$ sites for different x values; the peak around $M = 0.8$ is for the finite U sites whereas peak at lower M is for the induced moments ($M_{U=0}$) at $U = 0$ sites. Distribution of local moments for $U = 0$ and $U = 8$ sites separately at (b) $x = 0.4$ and (c) $x = 0.1$. (d) Structure factor $s(\pi, \pi, \pi)$ and induced moment ($M_{U=0}$) at $U = 0$ sites with x for $T = 0.02$ shows one to one correspondence between the onset of antiferromagnetic correlations and formation of induced magnetic moments at $U = 0$ sites. The induced moments mediate the antiferromagnetic correlation below classical percolation threshold limit.

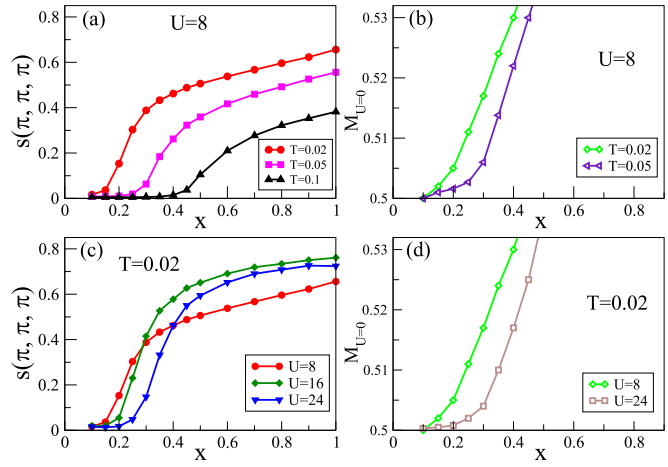

FIG. 7. (a) Structure factor $s(\pi, \pi, \pi)$ vs x for different temperatures show that the percolation threshold increases with temperature. (b) Comparison of the induced moment ($M_{U=0}$) at $U = 0$ sites with x between $T = 0.02$ and $T = 0.05$ for $U = 8$ case. (c) Structure factor $s(\pi, \pi, \pi)$ vs x for three different U values at $T = 0.02$. The percolation threshold increases with U values due to suppression of charge fluctuations at large U. (d) Comparison of the induced moment ($M_{U=0}$) at $U = 0$ sites with x between $U = 8$ and $U = 24$ cases.

peak at $M = 0.86$, implying uniform local moment magnitudes on all sites within the semiclassical calculation. As x is reduced, a new peak at lower M appears that indicates the moment formation at $U = 0$ sites. Figures 6(b) and 6(c) for $x = 0.4$ and $x = 0.1$, respectively, confirm this scenario. This also corroborates the data shown in Fig. 2(c) that shows the signature of induced moment on the uncorrelated ($U = 0$) sites. Just as seen in Fig. 2(c), here too we see that, if x reduces, the location of the new peak moves towards $M = 0.5$ signaling that the induced moment magnitudes get weaker. In addition, we note that the increase in the peak height at low M is simply due to increasing number of $U = 0$ sites as x approaches zero.

Correlating the low-temperature-induced M in the $U = 0$ sites with the AF order parameter in Fig. 6(d), we see a crucial fact that the long-range AF order between $U = 8$ sites depends on the existence of local moments at $U = 0$ sites. Induced moments at $U = 0$ sites are almost negligible up to $x = 0.15$ and the system remains paramagnetic. Beyond $x = 0.15$ the induced moments at $U = 0$ sites increase and as a result the system enters into an antiferromagnetic state at small x. This intimate relation between long-range AF order and induced moments in the $U = 0$ sites is central to the stability of the AF order below the classical percolation threshold. Above $x \approx 0.31$, while the cooperation continues to exist as discussed in context of Fig. 3, the AF order can stabilize by the usual percolation mechanism as well.

We now investigate the percolation threshold in two scenarios: (i) with temperature increase and (ii) at large U. The AF order parameter as a function of x is shown in Fig. 7(a) at three temperatures. While there is an overall suppression of the order parameter magnitude with temperature, we see that the critical x threshold for sustaining AF order moves towards higher values of x. To understand this, we reiterate that the long-range antiferromagnetic order in the diluted system arises from the cooperation between local moments at $U \neq 0$ and $U = 0$ sites. However, the induced magnetic moments on the $U = 0$ sites and antiferromagnetic correlations between them are weak, as seen from the small charge gap in the projected density of states in Fig. 4(c). Thus, with temperature increase, thermal fluctuations first suppress the induced moment magnitudes on the $U = 0$ sites. This phenomena is shown in Fig. 7(b), where we see that the local moments on the $U = 0$ sites are significantly reduced at higher temperatures. Once this order is lost, the only way long-range magnetic order can survive is by classical percolation between the large local moments on the $U \neq 0$ sites. That is why the structure factor in Fig. 7(a) shifts toward the classical percolation threshold with temperature increase. As shown in Fig. 7(c), the percolation threshold x_p also increases with U. At large, U charge fluctuations are suppressed, and the Heisenberg model accurately describes the Hubbard model. Thus, the crucial ingredient of induced moments on the $U = 0$ sites needed for stabilizing long-range magnetic order is systematically weakened at larger U value. This trend is seen in Fig. 7(d). The induced magnetic moment that mediates the AF order below x_p^{sc} values (for example induced moments at $U = 0$ sites for $x = 0.2$ and $U = 8$ case) are not induced at larger U values. As a result, the x_p increases with U and approaches the classical percolation threshold.

VI. CONCLUSIONS

We have employed a semiclassical technique to map out the temperature vs dilution phase diagram of the "diluted Hubbard model". Our method at low temperature is close to unrestricted Hartree-Fock method and become progressively

accurate with temperature. With increasing the temperature as a thermal fluctuation dominated phase is approached the method agrees quite well with DQMC as mentioned earlier. In the intermediate temperature (where we performed our calculations) the approximation is still better than simple Hartree Fock at finite temperature as was shown in Ref. [28]. Within this scheme we have shown that away from the weak-coupling ($U \ll BW$) and strong-coupling ($U \gg BW$) limit, dilution weakens the long-range magnetic order, but allows it to survive to dilution values much below the classical percolation threshold.

At low temperature, the Mott insulator at $x = 1$ evolves in to pseudogapped metal (for $x \leqslant 0.15$) by nontrivial spectral weight transfer phenomena that transforms the two Mott subbands into four sub-bands. Our analysis shows that in diluted regime the system has two distinct energy scales for charge excitations, one controlled by U and another emergent gap that arises out of weak local moment induced on the $U = 0$ sites. Such behavior of the density of states qualitatively agrees with DQMC studies in two dimensions [19]. By performing finite-size scaling analysis, we also show that the induced moments at the $U = 0$ sites and the $U \neq 0$ sites cooperate to form long-range magnetic order in the thermodynamic limit.

We further demonstrate that cooperation between the $U = 0$ and $U \neq 0$ sites is crucial to the magnetic order by showing that increasing U to large values, brings the critical percolation threshold to the classical value which requires system spanning AF patches exclusively made out of $U \neq 0$ sites. In addition by increasing temperature we have shown that the closure of the Mott gap by closing the smaller charge gap again disrupts the cooperation between the AF order between the two kinds of sites which pushes the percolation threshold to the classical values. This phenomenology is also seen in exact diagonalization where local Kondo coupling and Ruderman-Kittel-Kasuya-Yosida scales compete to control the magnetic properties of s-d models for carbon nanotubes [50] and broadly agrees with DQMC study on Lieb lattice [26].

ACKNOWLEDGMENT

We acknowledge use of the Meghnad2019 computer cluster at SINP.

APPENDIX: EFFECTIVE SPIN-FERMION HAMILTONIAN

We consider the following electron-hole symmetric (EHS) one band Hubbard Hamiltonian:

$$H = -t \sum_{<i,j>,\sigma} c^{\dagger}_{i,\sigma} c_{j,\sigma} + U \sum_{i} \left(n_{i,\uparrow} - \frac{1}{2}\right)\left(n_{i,\downarrow} - \frac{1}{2}\right),$$

where "t" is the nearest-neighbor hopping parameter and "U" denotes the on-site Hubbard interaction. We set $t = 1$ in our calculations.

After some trivial algebra and dropping a constant term the EHS Hubbard model becomes

$$H = -t \sum_{\langle i,j\rangle,\sigma} c^{\dagger}_{i,\sigma} c_{j,\sigma} + U \sum_{i} n_{i,\uparrow} n_{i,\downarrow} - \frac{U}{2} \sum_{i} n_i.$$

We denote the nearest-neighbor hopping term and the third term which is a one-body operator as H_0 and the second term which is the interaction term as H_1. We need to transform the interaction term as a combination of two quadratic terms to set up the Hubbard-Stratonovich (HS) decomposition formalism:

$$n_{i,\uparrow} n_{i,\downarrow} = \left[\tfrac{1}{4} n_i^2 - S_{iz}^2\right] = \left[\tfrac{1}{4} n_i^2 - (\mathbf{S}_i.\hat{\Omega}_i)^2\right]. \tag{A1}$$

Here $\mathbf{S}_i$ is the spin operator which is defined as $\mathbf{S}_i = \frac{\hbar}{2} \sum_{\alpha\beta} c^{\dagger}_{i,\alpha} \sigma_{\alpha,\beta} c_{i,\beta}$, $\hat{\Omega}$ is an arbitrary unit vector, σ are the Pauli matrices, and we take $\hbar$ to be 1. We use the rotational invariance of S^2_{iz}, i.e., $(\mathbf{S}_i.\hat{\Omega}_i)^2 = S^2_{ix} = S^2_{iy} = S^2_{iz}$.

The partition function for the Hamiltonian is $Z = Tre^{-\beta H}$, where β is inverse temperature $(1/T)$ (k_B is set to 1). Next we divide the interval $[0, \beta]$ into M equally spaced slices, defined by $\beta = M\Delta\tau$, separated by $\Delta\tau$ and labeled from 1 to M. For large M, $\Delta\tau$ is a small parameter and allows us to employ the Suzuki-Trotter decomposition, so that we can write $e^{-\beta(H_0+H_1)} = (e^{-\Delta\tau H_0} e^{-\Delta\tau H_1})^M$ to first order in $\Delta\tau$. Then, using the Hubbard-Stratonovich identity, $e^{-\Delta\tau U[\sum_i \frac{1}{4} n_i^2 - (\mathbf{S}_i.\hat{\Omega}_i)^2]}$ can be shown to be proportional to

$$\int d\phi_i(l) d\Delta_i(l) d^2\Omega_i(l) e^{-\Delta\tau\{\sum_i [\frac{\phi_i^2(l)}{U} + i\phi_i(l) n_i + \frac{\Delta_i^2(l)}{U} - 2\Delta_i(l)\hat{\Omega}_i(l)\mathbf{S}_i]\}}.$$

Here $\phi_i(l)$ is the auxiliary field for charge density and $\Delta_i(l)$ is auxiliary field for spin density and "(l)" is a generic time slice. Further we define a new vector auxiliary field $\mathbf{m}_i$ as the product $\Delta_i(l)\hat{\Omega}_i(l)$. Putting all of this back to the partition function we find the effective Hamiltonian. Now we make two approximations which make our model different from DQMC. First we drop the τ dependence of the Hamiltonian and we use the saddle-point value of $i\phi_i = \frac{U}{2}\langle n_i\rangle$. Last, by rescaling $\mathbf{m}_i \to (U/2)\mathbf{m}_i$ we find the effective Hamiltonian as

$$H_{\text{eff}} = -t \sum_{\langle i,j\rangle,\sigma} c^{\dagger}_{i,\sigma} c_{j,\sigma} + U/2 \sum_{i} (\langle n_i\rangle n_i - \mathbf{m}_i.\sigma_i) + (U/4) \sum_{i} \left(\mathbf{m}_i^2 - \langle n_i\rangle^2\right) - \frac{U}{2} \sum_{i} n_i - \mu \sum_{i} n_i.$$

The chemical potential μ is used to tune the global electron density equal to 1. In our calculation we have considered finite U at randomly chosen sites k with a concentration x and $U = 0$ at rest of the sites (concentration $1 - x$). We note that the HS transformation is a local transformation that decouples the many-body on-site interaction. It does not depend on whether other sites in the system are correlated. So, in the diluted limit ($x < 1$), the terms containing U are present only for the correlated sites (i.e., site with $U \neq 0$). The general Hamiltonian for the diluted case:

$$H_{\text{eff}} = -t \sum_{\langle i,j\rangle,\sigma} c^{\dagger}_{i,\sigma} c_{j,\sigma} + U/2 \sum_{k} (\langle n_k\rangle n_k - \mathbf{m}_k.\sigma_k) + (U/4) \sum_{k} \left(\mathbf{m}_k^2 - \langle n_k\rangle^2\right) - \frac{U}{2} \sum_{k} n_k - \mu \sum_{i} n_i,$$

where i, j run over all sites and k is assigned only for impurity sites.

[1] P. W. Anderson, Science **235**, 1196 (1987).
[2] S. Sachdev, Nat. Phys. **4**, 173 (2008).
[3] B. Keimer, S. A. Kivelson, M. R. Norman, S. Uchida, and J. Zaanen, Nature (London) **518**, 179 (2015).
[4] T. J. Liu, J. Hu, B. Qian, D. Fobes, Z. Q. Mao, W. Bao, M. Reehuis, S. A. J. Kimber, K. Prokes, S. Matas *et al.*, Nat. Mater. **9**, 718 (2010).
[5] C.-W. Liu, S. Liu, Y.-J. Kao, A. L. Chernyshev, and A. W. Sandvik, Phys. Rev. Lett. **102**, 167201 (2009).
[6] M. R. Norman, Physics **1**, 21 (2008).
[7] M. Kircan and M. Vojta, Phys. Rev. B **73**, 014516 (2006).
[8] A. L. Chernyshev, Y. C. Chen, and A. H. Castro Neto, Phys. Rev. Lett. **87**, 067209 (2001).
[9] M. Sato, S. Furukawa, S. Onoda, and A. Furusaki, Mod. Phys. Lett. B **25**, 901 (2011).
[10] L. Wang and A. W. Sandvik, Phys. Rev. Lett. **121**, 107202 (2018).
[11] B. Schmidt and P. Thalmeier, Phys. Rep. **703**, 1 (2017).
[12] Y. H. Szczech, M. A. Tusch, and D. E. Logan, J. Phys.: Condens. Matter **10**, 639 (1998).
[13] S. S. Singh Kunwar, A. Sen, T. Vojta, and R. Narayanan, Phys. Rev. B **98**, 024206 (2018).
[14] A. W. Sandvik, Phys. Rev. B **66**, 024418 (2002).
[15] A. Chakraborty, A. J. Epstein, M. Jarrell, and E. M. McCarron, Phys. Rev. B **40**, 5296(R) (1989).
[16] S. W. Cheong, A. S. Cooper, L. W. Rupp, B. Batlogg, J. D. Thompson, and Z. Fisk, Phys. Rev. B **44**, 9739(R) (1991).
[17] C. C. Wan, A. B. Harris, and J. Adler, J. Appl. Phys. **69**, 5191 (1991).
[18] O. P. Vajk, P. K. Mang, M. Greven, P. M. Gehring, and J. W. Lynn, Science **295**, 1691 (2002).
[19] M. Ulmke, P. J. H. Denteneer, R. T. Scalettar, and G. T. Zimanyi, Europhys. Lett. **42**, 655 (1998).
[20] A. Medhi, S. Basu, and C. Kadolkar, J. Appl. Phys. **101**, 09D504 (2007).
[21] J.-Y. P. Delannoy, A. G. Del Maestro, M. J. P. Gingras, and P. C. W. Holdsworth, Phys. Rev. B **79**, 224414 (2009).
[22] K. Christensen, *Percolation Theory* (Imperial College, London, 2002).
[23] K. Kato, S. Todo, K. Harada, N. Kawashima, S. Miyashita, and H. Takayama, Phys. Rev. Lett. **84**, 4204 (2000).
[24] A. L. Chernyshev, Y. C. Chen, and A. H. Castro Neto, Phys. Rev. B **65**, 104407 (2002).
[25] P. Carretta, G. Prando, S. Sanna, R. De Renzi, C. Decorse, and P. Berthet, Phys. Rev. B **83**, 180411(R) (2011).
[26] L. Oliveira-Lima, N. C. Costa, J. P. de Lima, R. T. Scalettar, and R. R. dos Santo, Phys. Rev. B **101**, 165109 (2020).
[27] N. D. Mermin and H. Wagner, Phys. Rev. Lett. **17**, 1133 (1966).
[28] A. Mukherjee, N. D. Patel, S. Dong, S. Johnston, A. Moreo, and E. Dagotto, Phys. Rev. B **90**, 205133 (2014).
[29] A. Mukherjee, N. D. Patel, C. Bishop, and E. Dagotto, Phys. Rev. E **91**, 063303 (2015).
[30] S. Kumar and P. Majumdar, Eur. Phys. J. B **50**, 571 (2006).
[31] K. Pradhan and S. Yunoki, Phys. Rev. B **96**, 214416 (2017).
[32] S. Chakraborty, S. K. Das, and K. Pradhan, Phys. Rev. B **102**, 245112 (2020).
[33] R. Blankenbecler, D. J. Scalapino, and R. L. Sugar, Phys. Rev. D: Part. Fields **24**, 2278 (1981).
[34] A. Georges, G. Kotliar, W. Krauth, and M. J. Rozenberg, Rev. Mod. Phys. **68**, 13 (1996).
[35] M. H. Hettler, M. Mukherjee, M. Jarrell, and H. R. Krishnamurthy, Phys. Rev. B **61**, 12739 (2000).
[36] G. Kotliar, S. Y. Savrasov, G. Palsson, and G. Biroli, Phys. Rev. Lett. **87**, 186401 (2001).
[37] T. Paiva, R. T. Scalettar, C. Huscroft, and A. K. McMahan, Phys. Rev. B **63**, 125116 (2001).
[38] H. Park, K. Haule, and G. Kotliar, Phys. Rev. Lett. **101**, 186403 (2008).
[39] L. Fratino, P. Semon, M. Charlebois, G. Sordi, and A. M. S. Tremblay, Phys. Rev. B **95**, 235109 (2017).
[40] K. Seki, T. Shirakawa, and S. Yunoki, Phys. Rev. B **98**, 205114 (2018).
[41] T. Sato and H. Tsunetsugu, Phys. Rev. B **94**, 085110 (2016).
[42] G. Rohringer, A. Toschi, A. A. Katanin, and K. Held, Phys. Rev. Lett. **107**, 256402 (2011).
[43] R. Staudt, M. Dzierzawa, and A. Muramatsu, Eur. Phys. J. B **17**, 411 (2000).
[44] P. R. C. Kent, M. Jarrell, T. A. Maier, and T. Pruschke, Phys. Rev. B **72**, 060411(R) (2005).
[45] N. D. Patel, A. Mukherjee, N. Kaushal, A. Moreo, and E. Dagotto, Phys. Rev. Lett. **119**, 086601 (2017).
[46] G. Jana and A. Mukherjee, J. Phys.: Condens. Matter **32**, 365602 (2020).
[47] R. Tiwari and P. Majumdar, Europhys. Lett. **108**, 27007 (2014).
[48] G. D. Mahan, *Quantum Many Particle Physics* (Plenum Press, New York, 1990).
[49] S. Kumar and P. Majumdar, Europhys. Lett. **65**, 75 (2004).
[50] Y. Luo, C. Verdozzi, and N. Kioussis, Phys. Rev. B **71**, 033304 (2005).